Numerical vs Experimental Sputtering Deposition Phase formation prediction in magnetron sputtered Cu(Ti)Zn thin films : Numerical vs Experimental approaches

Dimitri Boivin, Pascal Brault, Andrea Jagodar, Thomas Vaubois, Edern Menou, Barthélemy Aspe, Amaël Caillard, Pascal Andreazza, Marjorie Cavarroc, Anne-Lise Thomann

Phase formation prediction in magnetron sputtered Cu(Ti)Zn thin films : Numerical vs Experimental approaches

Dimitri Boivin,[1,2] Andrea Jagodar,[1] Pascal Brault,[1,3] Thomas Vaubois,[4] Edern Menou,[4] Barthélemy Aspe,[1] Amaël Caillard,[1] Pascal Andreazza,[5] Marjorie Cavarroc-Weimer,[4] and Anne-Lise Thomann[1]

[1)]*GREMI, UMR7344, CNRS-Université d'Orléans, 14 rue d'Issoudun, F-45067 Orléans, France*

[2)]*Nantes Université, CNRS, Institut des Matériaux de Nantes Jean Rouxel, IMN, F-44000 Nantes, France*

[3)]*MS4ALL, 1 avenue du Champ de Mars, F-45000 Orléans, France*

[4)]*Safran Tech, rue des jeunes bois, Châteaufort, CS 80112, F-78772 Magny-les-Hameaux, France*

[5)]*ICMN, UMR7374, CNRS-Université d'Orléans, 1 Rue de la Ferollerie, F-45100 Orléans, France*

(*Electronic mail: anne-lise.thomann@univ-orleans.fr)

(*Electronic mail: marjorie.cavarroc@safrangroup.com)

(Dated: 20 December 2024)

In this work we evaluated the ability of three numerical methods to predict the phase formation in Cu-Zn binary and Cu-Ti-Zn ternary alloy thin films deposited by DC-magnetron sputter deposition. Molecular dynamics simulations were carried out to simulate the growth of the alloy film and study the organization at the atomic level. A Machine Learning (ML) approach trained with a recently published bulk HEA (high entropy alloy) database was used to determine the presence of an amorphous phase, solid solutions or/and intermetallics. Finally, CALPHAD (CALculation of PHAse Diagrams) thermodynamic modeling based on Gibbs energy calculations allows to simulate the phase diagrams. This was done taking the experimental energy distribution functions of film forming species as inputs for the calculations. In this paper we discuss both agreements and limits of each method depending on their starting hypotheses and expected domains of validity. Crystalline phases formed in experimental films were investigated by grazing incidence X-ray diffraction (GIXRD). Comparison with CALPHAD results highlight that for pure Ti or binary Cu-Zn films, the thermodynamically stable phases are formed in the films. Less agreement was found at low or high percentage of Ti introduced in the Cu-Zn system, and drastic differences were observed for compositions close to equimolarity. In those cases, the out of equilibrium nature of the magnetron sputtering deposition technique is evidenced. The very limited agreement between GIXRD and ML approach is explained by the available database which is exclusively based on bulk alloys. Chemical composition of the alloy does not itself determine the stabilized phases: elaboration techniques are to be taken into account too. Molecular Dynamics (MD) simulations bring information on a possible segregation of the Zn element to the surface and grain boundaries. An interesting result is the very good agreement evidenced between the diffraction patterns calculated on the simulated films and that experimentally measured GIXRD

Keywords: Magnetron sputtering, Molecular Dynamics Simulations, Phase diagram, Machine Learning, CALPHAD

I. INTRODUCTION

Medium or High Entropy Alloys (MEAs, HEAs) or Complex Concentrated Alloys (CCAs) have attracted interest in the last decades for their original properties related to their chemical composition and structural characteristics. Several review papers on HEA bulk or coatings summarize the numerous studies published and highlight their outstanding association of properties[1–3]. In more recent works, antimicrobial HEA thin films have been synthesized by including active chemical elements like silver, copper, zinc etc. in the alloy composition[4,5]. The structure and phases of thin films control their antimicrobial characteristics. For instance, studies have shown the antiviral properties, especially on the SARS-CoV-2 virus, of binary and ternary alloys from the Cu-Zn, Cu-Ni, Cu-Ti, Cu-Ni-Zn etc. systems[6,7]. In 2021, Mostaghimi et al tested the effectiveness of Cu-Ni-Zn coatings in a hospital environment (on door handles, armrests, etc.) and proved that it significantly increased the duration of antibacterial activity while requiring less maintenance[8]. We can note that in his review, V. Govind mentions the strategy which consists in using families of more complex alloys, such as HEAs, in order to combine numerous functional properties.[6]. Such an approach is also pursued by Z. Li et al, with a Cu-based HEA: CuFeCrCoNi[5]. Because of the huge number of compositions to be investigated in these multi-elements materials, an exploration conducted purely experimentally would be excessively expensive and time-consuming. Many works have thus been devoted to find key physical or thermodynamic parameters, or define numerical approaches, that allow predicting the material structure (mainly Body Centered Cubic (BCC), Face Centered Cubic (FCC) or Hexagonal Close-Packed (HCP) solid solutions and intermetallics) and their degree of crystallinity as a function of the composition. Thermodynamic calculations have often been used to determine the stable phases that should form at equilibrium depending on the chemical composition and the operating temperature. In addition, multiple criteria have been defined including mixing enthalpy and entropy, elemental atomic size mismatch, electronegativity mismatch, etc. to better predict the stabilized structure and thus the final properties[9–11]. More recently, the use of data science tools from the field of artificial intelligence, and in particular the construction of machine-learned, data-based models, made possible to establish relationships between compositions and physicochemical properties to design new bulk HEAs with tailored properties[12]. The ability of data-based models, first principles calculations, and calculations of phase diagrams to solve the complex issue of designing optimal multi-element alloys for given applications has been discussed[5,13].

The aim of our work is to design and produce complex metallic alloy thin films by magnetron sputter deposition dedicated to antimicrobial applications. Since a degree of bacteria resistance has been reported for silver[14], copper was chosen in association to zinc to ensure bactericidal and antiviral properties by "release killing"[15]. Following a methodology based on the progressive increase of the alloy complexity, we have decided to start from the Cu-Zn system and study the evolution of the film structural and morphological properties when other elements, each expected to bring complementary properties (resistance to abrasion, hardness etc.) are added. In this paper we report on the Cu-Zn and Cu-Zn-Ti systems.

Our approach is based on the coupling of three numerical methods of phase formation prediction that will be compared to experimental data. In a first step, the CALPHAD (CALculation of PHAse Diagrams[16]) method will be employed to identify the stability domains of the various crystallographic phases based on the alloy chemical composition and on the deposition temperature. CALPHAD predictions will be compared to those of a machine learning model trained on bibliographic data available for bulk HEAs. In addition, since conditions of film deposition by magnetron sputtering are out of equilibrium compared to classical metallurgy, simulations by molecular dynamics will be carried out. In previous works, we have shown that these calculations allow the study of the film growth in conditions close to that of magnetron sputter experiments by using the energy distribution functions of each specie interacting with the substrate[17–19]. For instance, phase formation has been successfully anticipated in the case of a HEA thin film growth[20,21].

II. METHODS

A. Thin Film Synthesis & Physico-Chemical Characterization

The thin films were prepared in a stainless steel sputtering system made of a deposition chamber and an airlock. The system is equipped with three balanced 4-inch magnetron furnished with a titanium target (99.99 % purity), a copper target (99.99 % purity) and a zinc target (99.99 % purity). Argon flow rate is kept constant at 10 sccm and pressure at 0.5 Pa. Base pressure in the chamber is 10^{-6} mbar or lower as measured by a Pfeiffer Compact Full-Range pressure gauge. Pressure during deposition is measured by a Pfeiffer Baratron gauge and is controlled through a throttle valve between the chamber and the turbopump. A rotating substrate holder is located 11.5

cm away from the targets, facing the magnetrons, 30° tilted. All depositions were performed at room temperature.

Thin films were deposited for different sets of target powers ranging from 20-400 W. Cu/Zn ratio is kept close to equimolarity while Ti content varied from 3 to 76 %. Thin films were deposited on single-crystal silicon substrates (p-doped Si(100)) cleaned in an ultrasonic bath, 10 min in isopropanol and 10 min in ethanol. All depositions were performed for 10 min leading to film thicknesses comprised between 400-900 nm depending on the deposition parameters.

The thin film crystallographic structure was determined by Grazing Incidence X-Ray Diffraction (GIXRD) using an AXS Bruker D8 Advance diffractometer with the Cu K_α radiation (λ = 0.15406 nm). XRD measurements were performed between 20° and 80° at a 1° grazing incidence. Thickness and morphology were determined using a Zeiss Supra 40 Field Emission Gun-Scanning Electron Microscopy (FEG-SEM) operating at 3 kV. In addition, Energy X-ray Dispersive Spectroscopy (EDS) is carried out on 200 × 200 µm surface areas, using Ti 4.512 keV and 0.452 keV rays, to estimate the thin film mean composition. EDS results were compared to Rutherford Backscattering Spectroscopy (RBS) results measurements for four samples. RBS, performed at the CEMHTI[22] laboratory on a Pelletron accelerator with 2 MeV alpha particles (with 166° scattering angle), allowed in-depth composition homogeneity assessment. RBS analysis was performed on thinner thin films than those used for EDS, in order to properly quantify only Ti content, as both Zn and Cu feature close atomic weights. Spectra simulations were carried out with the SIMNRA software[23].

B. Molecular Dynamics simulations

Molecular Dynamics (MD) simulations based on the Newton equations of motion were implemented to describe the growth of alloy thin films at the atomic scale. The Embedded Atom Method (EAM) is chosen for describing Cu, Ti and Zn interactions[24]. Cross interactions make use of Johnson mixing rule[25,26]. The silicon substrate atoms interact by Tersoff potential[27], while Cu, Zn and Ti interactions with Si are described using Lennard-Jones potential[28,29] with Lorenz-Berthelot mixing rule.

The simulation box is composed of a silicon substrate with sizes 7.6 x 7.6 x 4.35 nm^3 for Cu-Zn films and 5.43 x 5.43 x 4.35 nm^3 for Cu-Ti-Zn films. Both sizes gave identical results in terms of phases and diffraction patterns for Cu-Zn. The first two bottom layers of Si atoms are fixed

for preventing substrate motion upon impact of depositing atoms. The remaining substrate atoms are subjected to Langevin thermostat at 300 K with 100 fs damping time to properly disspate the excess energy transferred by the fast-depositing atoms. A set of 10 atoms among Cu, Zn, Ti, in accordance with the targeted film composition, was periodically released towards the surface every 40000 timesteps. The timestep is 0.5 fs. The atoms were randomly placed at a height of 1.5 nm above the substrate. This height was increased by steps of 0.5 nm every 40000 timesteps in order to stay non interacting with the growing film.

The initial velocities of silicon atoms were randomly chosen in a thermal distribution at 300 K. In order to best imitate the experiments, the initial velocities of Cu, Ti and Zn were randomly chosen in a distribution matching the deposition conditions, following a procedure described previously[17,19,30]. The sputtered atom energy distribution was evaluated using the SRIM software[31] with sputter argon ion energy corresponding to the experimental target bias voltage. This SRIM-deduced energy distribution function wass then modified by the collision encountered with the gas atoms during the transport from target to substrate. For each targeted composition, 10000 atoms were released towards the surface. The total elapsed simulation time for each run was 20 ns. Simulations were carried out using the LAMMPS software[32,33]. X-ray diffraction patterns were calculated using the Debye method included in LAMMPS[34]. Snapshots were plotted using OVITO software[35]. The crystalline phases of the simulated films were identified using the Polyhedral Template Matching method implemented in OVITO.

C. Machine Learning

A machine learning classifier model for structure prediction was trained based on recently published data related to bulk HEAs[36]. It uses Gradient Boosting as implemented in the xgboost R library[37]. Since the database contains alloys of Cu, Ti and Zn, it provides some experimental basis to the model. Taking alloy composition (element nature and concentration) as input, the model predicts, similarly to the work of Lee et al.[36], seven structure classes: single solid solution (BCC, FCC or HCP), intermetallics, mix of BCC/FCC solid solutions, multiple phases (mixture of one or several solid solutions and one or several intermetallics), or amorphous phase(s). A precision similar to that of the work of Lee *et al.*[36] was attained (see its Supplementary Table 3), with a testing accuracy of approximately 84 % (*i.e.*, 84 % of structures correctly classified).

D. Calculation of Phase Diagrams

CALPHAD is a thermodynamic modelling method based on Gibbs energy calculations to simulate phase diagrams[16]. In this work, thermodynamic calculations were performed in the CALPHAD framework using the TCHEA6 database and version 2023a of the Thermo-Calc software[38]. These calculations enabled us to identify the phases that are expected stable in the ternary system Cu-Ti-Zn under equilibrium conditions.

III. RESULTS

A. Experimental Results - Thin Films Composition, Morphology and Microstructure

Experimental thin film compositions, as determined using EDS and RBS, are reported in Table I. The composition is a crucial parameter off complex metallic alloys driving the in-use properties, including the antibacterial activity as shown in the literature[39–41]. Similarly, it has been found to play an important role on the mechanical and physicochemical properties such as the hardness or the corrosion resistance[40]. By EDS, as shown in Table 1, we obtained the mean composition of the deposited films. However, since no in-depth resolution is accessible by this method, we used RBS measurements on three compositions. It was thus necessary to deposit thinner films, which has been done for 3, 10 and 24 at. % of Ti. With RBS analysis it is possible to discriminate elements in function of their weight. Zn and Cu being too close in the periodic table, their respective signals cannot be separated, but the Titanium peak is exploitable, and we obtained its atomic percentage with a precision of about 2 at. %. It is shown in the Table I that for the three samples the results are in good agreement with the EDS measurements within 2 % error. Moreover, from RBS results we checked that the alloy composition is constant over the entire thickness of the films. From these cross-analyses, we deduce that confidence can be established in the EDS measurements.

SEM surface and cross-section images are shown on Figure 1, and correspond to samples described in Table I SEM images for 37 at. % Ti contents are very close to those at 24 at. % Ti and thus 37Ti image is not shown for clarity. Surface images of Cu-Zn binary alloys (left side) present two topographies. The $Cu_{41}Zn_{59}$ alloy film (B1) features angular and faceted grains that are larger 100-200 nm than those of the $Cu_{61}Zn_{39}$ alloy film (B2) (smaller than 40 nm). The corresponding cross-section image of B1 reveals a columnar structure typical of magnetron sputtered thin films,

TABLE I. Composition at. % of the binary (B) and ternary (xTi) coatings measured by EDS and RBS. The ratio $\frac{\text{Cu}}{\text{Cu}+\text{Zn}}$ calculated from EDS results is also given.

	EDS			RBS			$\frac{\text{Cu}}{\text{Cu}+\text{Zn}}$
Sample	Cu	Ti	Zn	Cu	Ti	Zn	
B1	41	0	59	-	-	-	41 %
B2	61	0	39	-	-	-	61 %
3Ti	41	3	56	41	3	56	42 %
10Ti	46	10	44	44	9	47	51 %
24Ti	38	24	38	41	20	39	50 %
37Ti	35	37	28	-	-	-	56 %
42Ti	33	42	25	-	-	-	57 %
76Ti	13	76	11	-	-	-	54 %

as widely reported in literature[42,43]. The $Cu_{61}Zn_{39}$ alloy (B2) cross-section morphology presents a very different structure, exhibiting three layers. The first layer from the substrate is about 100 nm thick and has a columnar structure, as B1, with thinner columns. The second layer is about 800 nm thick and shows a porous and foam-like structure (nanocorals)[44]. The top layer is relatively dense and us about 100 nm thick.

With 3 at. % Ti addition (3Ti), the sharp faceted structure of B1 is somewhat preserved, while a messier cross-sectional columnar structure is visible. Higher titanium contents (10Ti, 24Ti, 42Ti) lead to the degradation of the crystallinity as the grain morphology becomes rounder and the grain size decreases. The columnar structure disappearance and the denser structures evidenced by cross-sectional views confirm progressive amorphization.

The $Cu_{13}Ti_{76}Zn_{11}$ (Ti76) alloy film surface features irregular patterns. The cross-section image exhibits a mix of columnar and vein-like structure, of around 1.4 µm thick. The structure seems to be finer when moving towards the film surface.

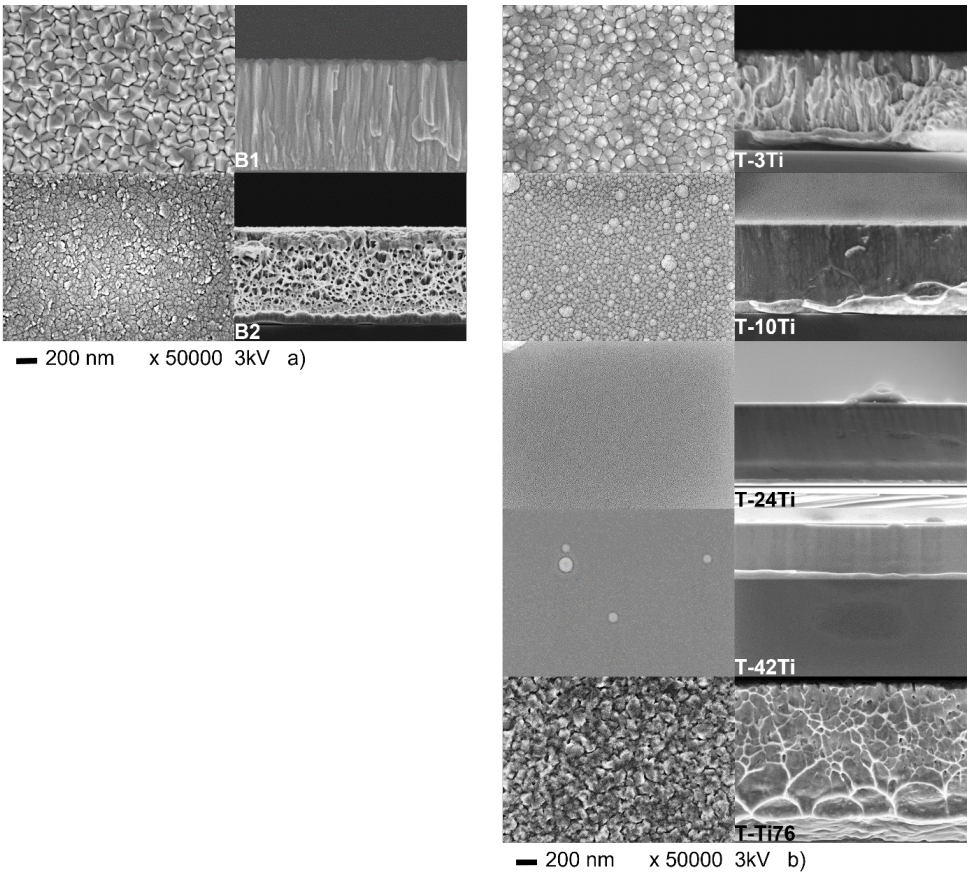

FIG. 1. SEM images of the plan views and cross-sections of a) the binary (B1 and B2) and b) ternary films (3Ti, 10Ti, 24Ti, 42Ti and 76Ti.

X-ray diffraction patterns for binary and ternary films, as well as that of pure Ti film, are shown in Figure 2. The B1 film ($Cu_{41}Zn_{59}$ alloy) contains one single phase as all the observed peaks match those of the γ-Cu_5Zn_8 phase. (BCC, JCPDS# 01-071-0397[45]. Please note, further call to ICCD/JCPDS/COD sheets will refer to Kabekoddu *et al*[45]) The diffraction pattern of the B2 film ($Cu_{61}Zn_{39}$ alloy), matches the peaks of a Zn-enriched α-Cu phase. (FCC, JCPDS#00-050-1333) with a composition of $Cu_{64}Zn_{36}$. This structure is a face-centered cubic phase with space group Fm3-m However, due to their close atomic radii, the lattice parameter of the α-Cu phase does not vary much with zinc additions. Therefore, the presence of other phases such as a solid solution of Zn, cannot be ruled out.

The diffraction pattern of the 3Ti film is similar to the B1 film, with a slight shift of diffraction peak angles (approximately -0.5°) indicating a variation in lattice parameters probably caused by a solubility of titanium in the γ-Cu_5Zn_8 and the disappearance of several peaks (between 45 and 60

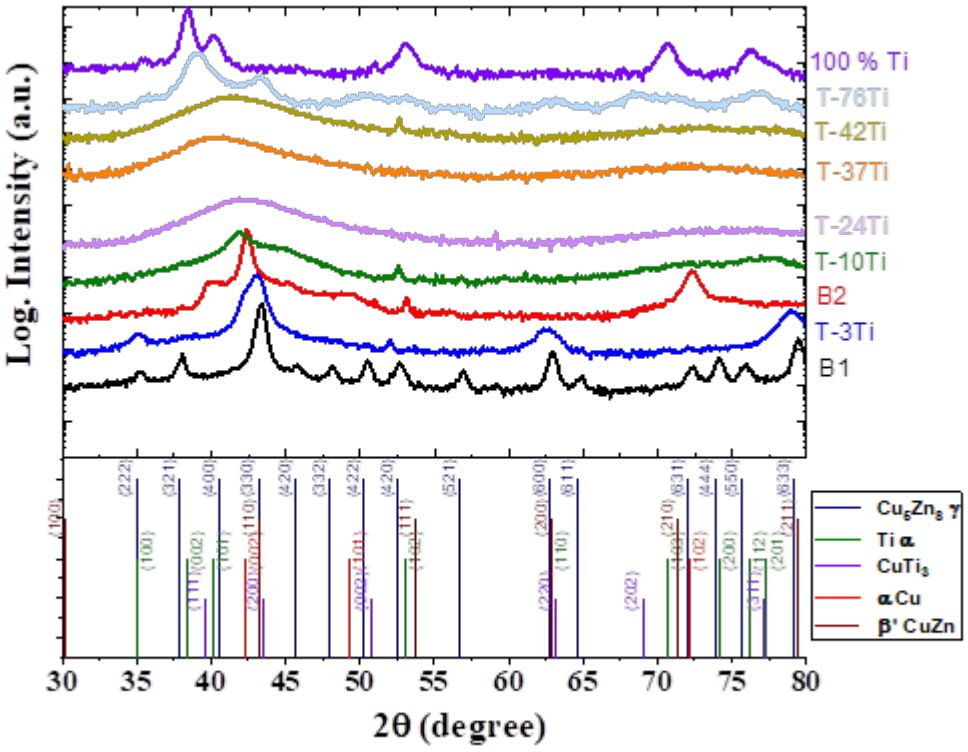

FIG. 2. GIXRD experimental patterns of the thin films. Note the log scale used for a better overview of the general shape of the all diffractograms. Positions of some expected peaks are indicated below the GIXRD patterns.

and between 70° and 75°). The widening of the peak and its asymmetry can also be explained by the formation of another phase such as β-CuZn phase. (BCC, JCPDS#04-003-4270) which three peaks lie at the same position as the main ones of the γ-Cu_5Zn_8.

The diffractogram of the 10Ti film displays three main very broad peaks: an asymmetrical peak at 41.6° and two wide peaks between 70-80°. The asymmetry of the peak located around 41° tends to indicate that more than one phase is present. The positions could correspond to shifted main peaks of α-Cu ($Cu_{64}Zn_{36}$) and γ-Cu_5Zn_8 phases or even of the β'-CuZn. Note that the small and thin peak at 52.6°, that appears randomly on the patterns, is attributed to an artefact of measurements.The general shape of the diffraction pattern points out a loss of crystallinity.

This trend is confirmed on the 24Ti and 42Ti films, which patterns exhibit a very broad peak at 42°, typical of an amorphous or nanocrystalline phase. This is in agreement with the SEM observations where a dense and smooth film is visible.

However, the 76Ti film is entirely crystalline with a pattern indicating the presence of at least two phases. By comparing to the ICCD database, the presence of a mixture of α-Ti (HCP, COD#9016190) and $CuTi_3$ (COD#15246555) phases is suspected. The width of the most intense peak, located below 40°, suggests a combination of contributions from oriented peaks (002) at 38.42° and (101) at 40.17° from α-Ti, but also from the most intense $CuTi_3$ oriented peak (111) at 39.6°. The peak at 43.49° corresponds to the (200)-oriented $CuTi_3$ peak. The other peaks from the diagram also correspond to the combination of contributions from the α-Ti and $CuTi_3$ phases.

The pure titanium thin film diffractogram indicates that the main present phase is the α-Ti phase.

B. Numerical method results

1. Molecular Dynamics Simulations of the film growth

Figure 3 displays the snapshots after 20 ns deposition time for all investigated compositions in the Cu-Ti-Zn system. Displayed compositions match the experimental film compositions. It can be observed that Zn concentrations are systematically slightly lower than those in the targeted compositions, the balance being Cu and Ti concentrations. This deviation to the targeted composition is only 1-2 %, lying in the uncertainty range of experimental methods. For the two binary alloys $Cu_{40}Zn_{60}$ and $Cu_{62}Zn_{38}$, Cu and Zn are clearly segregated into different, more or less tortuous, regions with their respective stable crystalline structure, *i.e.*, FCC and HCP respectively, at ambient temperature.

In alloys $Cu_{42}Ti_3Zn_{55}$ and $Cu_{48}Ti_9Zn_{43}$, Zn remains segregated in an HCP phase while a disordered Ti-enriched FCC Cu phase develops. At 9 % Ti, the FCC/HCP phase ratio is significantly reduced as Cu atoms moves in HCP structure. Low level of FCC Cu phase is observed corresponding to nearly isolated atoms. This is a limitation of Polyhedral Template Matching method that only takes into account the first neighbor environment of atoms. A change of behavior occurs for higher Ti additions with a transition, between 10 and 24 % Ti. The FCC phase changes to either a Cu-enriched Ti BCC phase or a CuTi BCC intermetallic compound (also determined on isolated atoms), whereas BCC phase was not present for low % Ti. It should be also noted that numerous

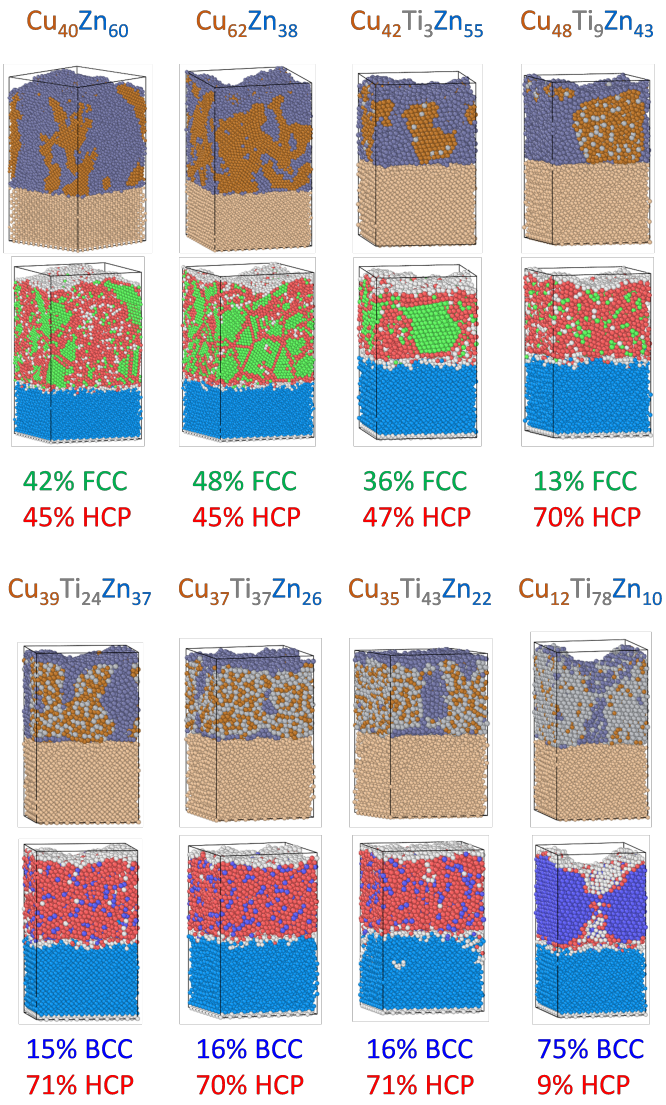

FIG. 3. Results from MD simulations. Color coding: brown Cu, light grey Ti, dark grey Zn, light brown Si substrate. 1st and 3rd row display the snapshot of each film which atomic composition is shown at the top $Cu_x(Ti_y)Zn_z$. 2^{nd} and 4^{th} rows display colored regions corresponding to phase structures (green FCC, blue BCC, red HCP, light grey unattributed (disordered) structure, light blue diamond phase of the silicon substrate). The crystalline phase ratios are displayed below the corresponding snapshots. The balance corresponds to disordered regions.

Cu atoms are then in HCP position. The predominant phase remains HCP and the secondary one (also including isolated atoms) turns from FCC to BCC.

For deeper insight into the crystallographic structure, the XRD patterns are simulated using the Debye method included in the LAMMPS software. Figure 4 displays the XRD patterns of the

films presented in Figure 3 . Binary films simulated XRD patterns are consistent with Zn-enriched α-Cu ($Cu_{64}Zn_{36}$) ICCD sheet. This could appear counterintuitive, since MD suggests Cu and Zn segregation. This is attributed to the similarity of atomic radii between copper and zinc, leading to a diffraction of a zinc-enriched copper solid solution similar to that of a mixture of two distinct copper and zinc solid solutions. Increasing amounts of titanium trigger phase transformations from HCP+FCC for low Ti contents to HCP+BCC and almost only BCC at the highest Ti content as shown in Figure 3. MD simulations predict the disappearance of the 42.3° and 49.3° peaks and the formation of a 39.2° peak matching the BCC β-Ti phase (Im3-m symmetry, sheet #mp-73 from the Materials Project database[46,47]) for the 76Ti alloy. The comparison between experimental and simulated patterns is discussed further below.

2. Structure Prediction with Machine Learning

A structure diagram of the Cu-Ti-Zn system , computed using the machine learning model, highlights the existence of solid solution or multiphase domains, as illustrated on Figure 5. The diagram is built through a complete mapping of Cu-Ti, Cu-Zn, Ti-Zn and Cu-Ti-Zn alloying systems with each element content ranging from 0-100 % with a variation step of 2.5 %, using data on bulk HEAs. A projection of the experimental compositions on the diagram predicts the formation of a single FCC phase for Ti contents ranging from 10-42 at. %. Composition of 3Ti and B1 samples lie in a domain where a mixture of solid solutions and intermetallics (MP) is expected, whereas composition of B2 and 76Ti is at the frontier between a single FCC or BCC phase domain, respectively and a multiphase domain. No composition lies in the very limited amorphous domain (AM).

3. Phase Prediction with CALPHAD

The calculated binary phase diagram, along with the thin film compositions obtained in this work, are presented in Figure 6. Cu-Zn diagram is in good agreement with the published experimental data and the most recent CALPHAD assessments[48–52]. Zn exhibits a large solubility in

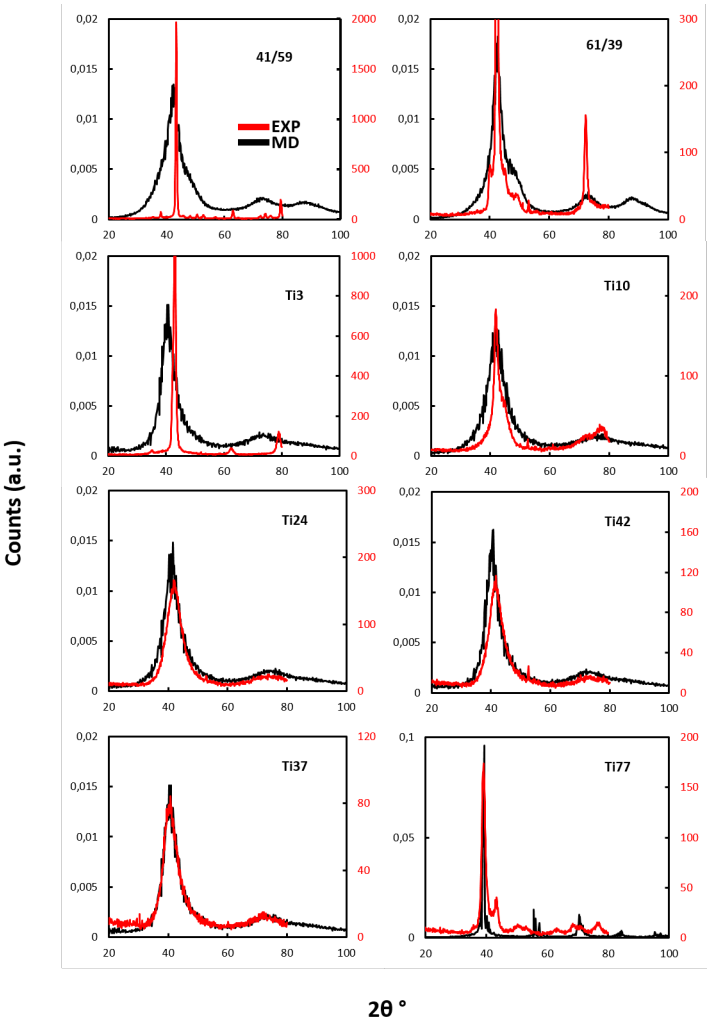

FIG. 4. Simulated X-ray patterns of the MD films reported in Figure 3, superimposed on the corresponding experimental GIXRD patterns of Figure 2.

the FCC copper solid solution, up to 36 at. % at 400°, while the HCP zinc solid solution can only accommodate up to 2 % Cu. Several intermetallic phases are reported on the phase diagram, respectively β (BCC), γ-Cu_5Zn_8 (FCC), ε (HCP) and δ (BCC). Below 450°, a second order phase transition occurs in the β phase leading to the formation of the ordered β' (BCC) phase (prototype: CsCl).

The 300 °C isothermal section of the ternary Cu-Ti-Zn system is presented in Figure 7 along with the deposited compositions. These compositions are located in different phase regions, thus we expect the coatings to display different phase equilibria. We can see that many of them contain a

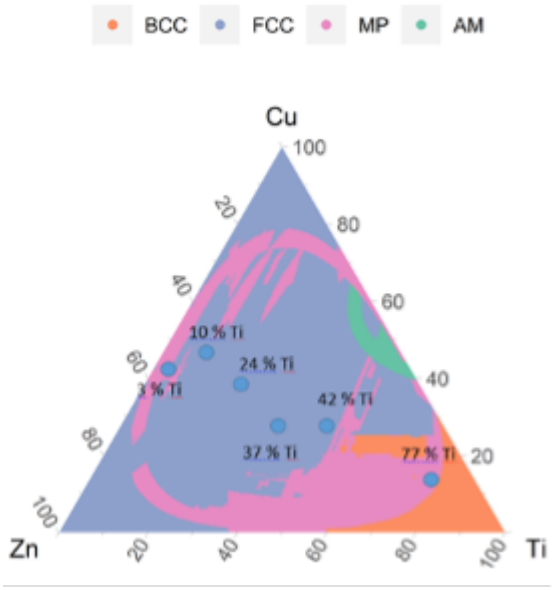

FIG. 5. Prediction of phase domains using the machine learning approach described in Section II C for the binary and ternary alloys. Blue dots correspond to experimental compositions. BCC and FCC labels define domains where a single solid solution of said structure is expected, while MP and AM labels respectively define domain of mixed phases formation or amorphous phase formation.

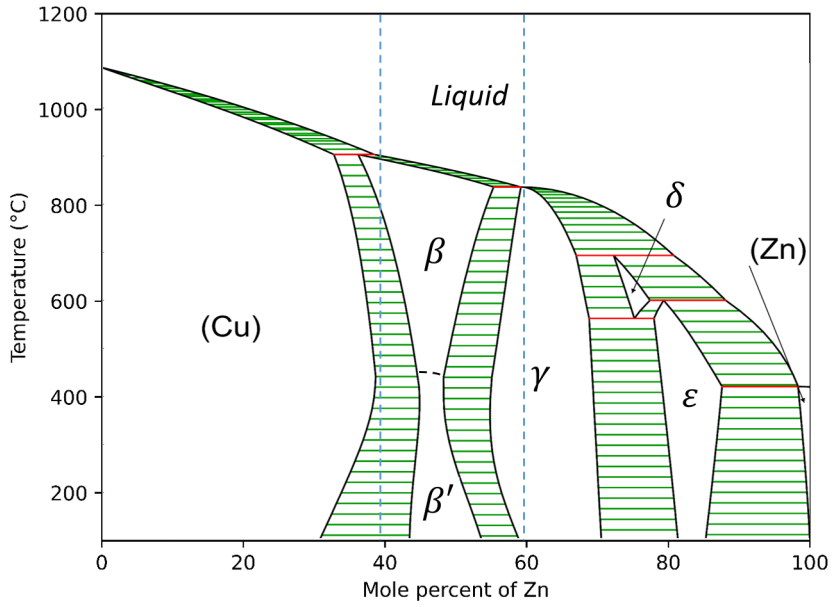

FIG. 6. Copper-Zinc phase diagram calculated using the TCHEA6 database and the Thermo-Calc software. Vertical dotted lines represent the experimental compositions (B1 and B2) reached in this work.

varying amount of the β' phase (BCC) in equilibrium with Ti-Cu binary phases. For the Ti-richest coating, thermodynamic calculations predict an equilibrium between pure hexagonal titanium and a Ti_2(Cu,Zn) compound. It is interesting to note the large solubility of titanium in theβ' phase, as the stability of this phase goes from the Cu-Zn binary section up to the Cu-Ti binary section.

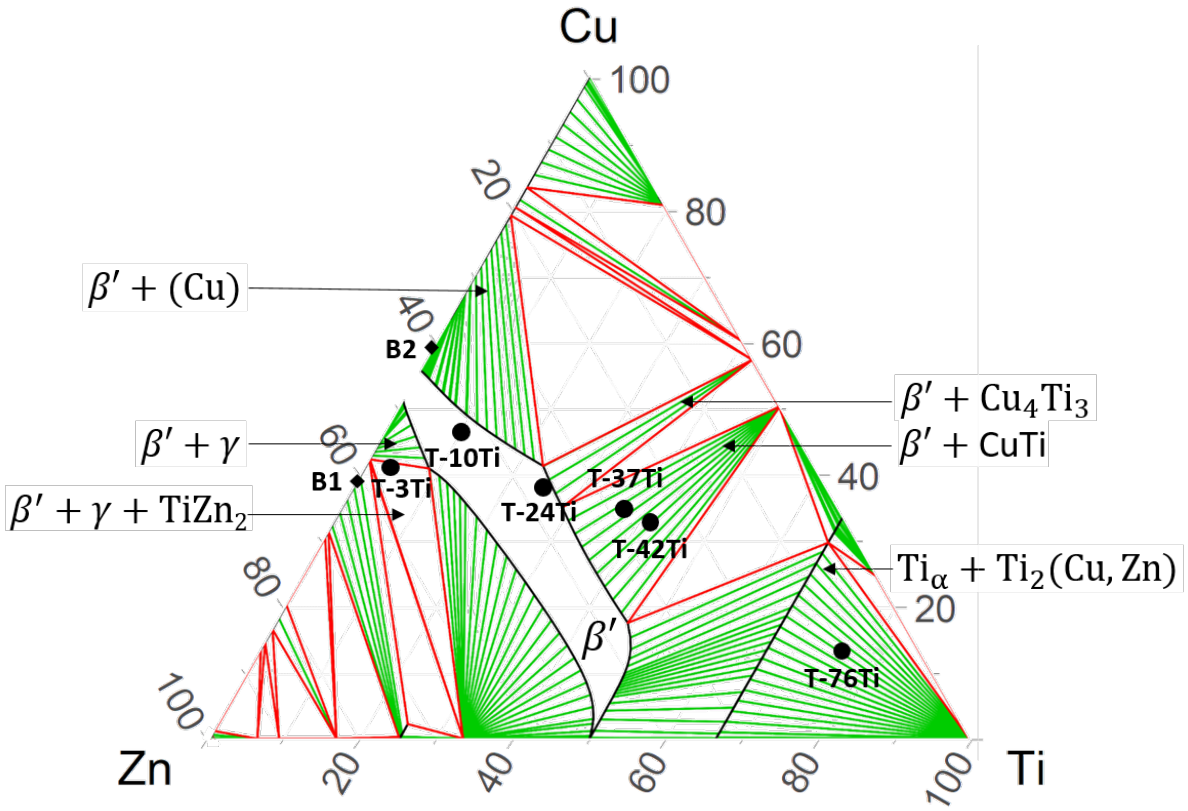

FIG. 7. Isothermal section at 300 °C of the Cu-Ti-Zn phase diagram calculated using the TCHEA6 database and the Thermo-Calc software. The black dots indicate the coating compositions reached in this work.

IV. DISCUSSION

A. CuZn

From experimental GIXRD (Figure 2) it is seen that the structure of Cu-Zn alloy greatly depends on the composition close to the equimolarity. Since deposition conditions were the same, except only for applied power on targets for reaching targeted compositions, we can state that the

TABLE II. Comparison between phases predicted by Machine Learning, CALPHAD calculations, Molecular Dynamics simulations and experimental determination by GIXRD.

Method	Ti	B1	B2	3Ti	10Ti	24Ti	42Ti	76Ti
GIXRD	α-Ti	γ-Cu_5Zn_8	α-Cu	γ-Cu_5Zn_8	γ-Cu_5Zn_8 + β-CuZn	Amorphous or nano-cryst.		α-Cu +Cu_3Ti
	HCP	BCC	FCC	BCC	FCC + BCC ?	Amorphous or nano-cryst.		HCP + ?
CALPHAD	α-Ti	γ-Cu_5Zn_8	α-Cu + β'	γ-Cu_5Zn_8 + β'	β'		β' + CuTi	α-Ti + Ti_2(Cu,Zn)
	HCP	BCC	FCC+BCC	BCC + BCC	BCC		BCC + BCT	HCP + BCT
ML	BCC	MP	FCC	MP	FCC			MP
MD	α-Ti	α-Cu + Zn-HCP		Cu(Ti)-FCC+Zn-HCP		Cu(Ti)-HCP+Zn-HCP		β-Ti(Cu)
	HCP			FCC+HCP		BCC+HCP		BCC

formation of the Zn-enriched α-Cu (FCC) or γ-Cu_5Zn_8 (BCC) phase is only related to the proportion of Cu and Zn in the film.The appearance of the γ phase (BCC) for B1 at the corresponding composition range is expected from thermodynamics (Figure 6) at relatively high temperature (600 °C), but is not predicted from MD simulations, operated at room temperature. XRD pattern calculated from MD (Figure 4) highlights a FCC phase, whose peaks are shifted from α-Cu phase due to the Zn enrichment, and are in complete accordance with the ICCD file of a $Cu_{64}Zn_{36}$ alloy. The same phase is predicted by MD for the B2 film which is, in this case, in quite good agreement with experimental GIXRD, (B2 lies close to the frontier between pure α-Cu and coexistence of α-Cu and β'-CuZn (BCC) phases domains) and machine learning (close to FCC solid solution domain). These contradictory data for B1 film suggest that the interaction potential used in MD is unable to predict the formation of this particular γ-Cu_5Zn_8 phase. EAM potentials are not parametrized to form this structure. Thus, in the present simulation conditions, MD will only be valid when the alloy composition leads to the stabilization of the Zn-enriched α-Cu (FCC) phase.

From the above results, predictions from CALPHAD appear in rather good agreement with experimental data. This would suggest that the energetic conditions of deposition, in our case, enables the formation of equilibrium phases. It is interesting to note that the machine learning model also shows its limitation for B1 sample, predicting the presence of multiple phases where experimental results show a single BCC phase.

B. CuTiZn Thin Films

The relative proportion of Cu and Zn is given for all films in Table I to guide the interpretation of the results. Comparison between experimental results and thermodynamic calculations shows a

partial agreement for the 3Ti sample (42 at. % of Cu, close to the value in B1), since the presence of the γ-Cu_5Zn_8 phase is predicted and observed. Films with a content of titanium between 10-42 at. % clearly lose their crystallinity and GIXRD results evidence low ordered, nano-sized phases or amorphous domains. This shows that Ti addition disturbs the formation of crystalline phases in the films, whereas for binary alloys (and at very low content of Ti) thermodynamically favorable phases are formed, even in the low energy conditions of magnetron sputter deposition. From 10-42 at. % Ti content, the non-equilibrium nature of the magnetron sputter deposition technique, which can be considered as a quenching process, is thus evidenced. This is the reason for the enhanced glass forming ability usually observed in multielementary alloy thin films deposited by this technique[41,53,54]. The machine learning approach predictions anticipates the formation of a FCC solid solution for 24Ti and 42Ti that is not observed experimentally.

For the titanium-richest thin film, the crystalline structure is in agreement with the ML approach (mixed phases domain) and partially matches the CALPHAD predictions which anticipate the formation of α-Ti + Ti2(Cu,Zn) phases (cf. II), in accordance with those evidenced by GIXRD.

C. Ti Thin Film

The experimental GIXRD diffractogram shows the presence HCP α-Ti titanium phase (Table II), as expected for magnetron sputtering deposition[55,56]. Both CALPHAD calculations and MD simulation predict the formation of the α-Ti phase, thus in agreement with the present experiments. On the contrary, ML fails in predicting the phase formed in pure Ti film, as a BCC β-Ti structure is expected. At low temperature, α-Ti is the most stable phase as indicated by CALPHAD, while the β-Ti phase is more common at high temperature as well as film with additional elements[56]. The limitation of the ML prediction may be related to the fact that the training database is built on binary and ternary alloys, without including pure elements.

D. Numerical methods *vs* experiments

All the above results on binary and ternary alloys support that, depending on the alloy composition (complexity of the system), CALPHAD calculations can anticipate the formation of the crystallized phases in sputtered thin films. This point has already been reported by Keuter *et al.* who states that thin-film phase formation is closer to (at least para-) equilibrium than has often

been assumed[57]. One of the sources of uncertainty when comparing CALPHAD predictions to experimental results lies in the choice of the temperature of the system. In our case we decided to use thermodynamic calculations at 300 °C for the ternary alloy. This value was estimated not too far from the experimental conditions, while ensuring accurate predictions. However, as mentioned above, the exact temperature inside the growing film is not known. A difference between the estimated temperature and the real value could partially explain discrepancies between simulations and experimental results. Moreover, one must keep in mind the paramount importance of the databases used to perform CALPHAD calculations. For instance, in their investigation of phase formation and thermal stability of sputtered AlSiTaTiZr high-entropy alloy thin films, Cemin *et al.* invoke the lack of updated databases for Si containing compounds which weakens the phase prediction in these systems[58]. In our case, the ternary system Cu-Ti-Zn is rather well known and the description is well implemented in the TCHEA6 database, therefore a good quality of predictions can be expected for equilibrated systems.

In literature it is shown that when the number of elements rises, predictions by CALPHAD may not be valid anymore for thin films. Cemin *et al.* systematically found disagreement between experimental results and predictions in their range of compositions for the AlSiTaTiZr alloy[58]. They explain the formation of a metastable phase by the extremely fast cooling rates reached in magnetron sputter deposition (non-equilibrium nature), in agreement with our conclusion. They infer that phase formation and selection in complex alloy thin films is determined by both thermodynamic and kinetic factors. They also emphasized that despite this conclusion, deeper thermodynamic investigations should continue in thin film literature of HEAs. For instance, Chang *et al.* developed a model based on experimental and theoretical research coupling DFT and CALPHAD calculation in order to take into account atomic diffusion at the surface, that means kinetic processes, and to predict phase formation in thin films of CuW and CuV.

Data obtained with ML (Figure 5, Table II)only allows identifying the presence of a mixture of phases, an ordered solid solution (BCC or FCC) or an amorphous phase. What can be observed, first on Figure 5, is that 3Ti and 76Ti lie in composition domains where a multiphase system is expected. This is what is evidenced by GIXRD for 76Ti, whereas a single phase is present for 3Ti. For 10-42 % Ti, FCC solid solution is predicted by ML, corresponding to the range of composition leading to the synthesis of poor crystallinity thin films. There is thus an accordance in the composition domains and frontiers, but the predictions do not match the experimental results. At this step, one has to remind that database accessible to perform such ML calculations are dedicated to bulk

alloys elaborated by metallurgical routes, usually including a quenching step in order to stabilize metastable phases. Thus, even if elaboration routes of bulk HEA are usually out of equilibrium, they are far from that of magnetron sputter deposition. The above observations clearly confirm that using this approach with such databases, is not accurate enough for the prediction of phase formation in sputtered films. This has been investigated by several groups on different alloys[59]. They were able to define domains of agreement but clearly come to the same kind of conclusion. Implementing such a method for PVD techniques would require building specific databases from data available in literature on thin films.

MD simulations are expected to best match experimental results since they describe the motion of atoms and organization at the atomic scale and also, here, because the energy distributions functions of incoming atoms have been used. Unfortunately, as explained above, the Cu-Zn system tends to form a very stable BCC phase (γ-Cu_5Zn_8, at a precise composition), that EAM interaction potentials used for Cu and Zn do not predict. This is the reason why GIXRD of 3Ti sample does not correspond to the simulated one (Figure 4). However, the experimental conditions used in the present work to obtain a content of Ti higher than 10 %, leads to a Cu/Zn proportion (Table I) far from the γ-Cu_5Zn_8 domain of stability as defined by CALPHAD (Figure 7). We think that this leads to a "α-Cu (FCC) type phase organization" in the films. This could explain the excellent agreement found from 10Ti to 42Ti in the position of the broad peaks present on both experimental and MD diffraction patterns.

Thus, MD simulations reproduce quite well our diffraction experimental results. Previously a good agreement was found in the case of high entropy alloy thin films[21]. Intrinsically the diffracting volume is very limited in MD simulations, leading to a lack of long range order and thus to broad peaks. It is shown from the snapshots that the films are crystallized at this atomic scale. From GIXRD analysis, we cannot check whether this nano-organization exists in the films. In the range between 10 to 42 at.% the crystalline structure calculated from MD data is mainly HCP (Figure 4) and this phase exists both, in the Zn and CuTi zones. This highlights the formation of a "collective" structure including all the elements, even if segregation of Zn atoms is observed at all the compositions. Experimentally we have no evidence of such a behavior of Zn. GIXRD cannot help since, as mentioned above, peaks listed in the α-CuZn phase JCPDS file fit exactly those of α-Cu (FCC) and Zn HCP coexisting nano-phase, as calculated by MD. However, one must keep in mind that CALPHAD has not predicted the coexistence of Cu and Zn separated phases, neither the formation of a HCP phase, whereas the stabilization of a CuTi phase in a certain range of

composition is anticipated by both techniques.

Again a recovery of a kind of order is visible in 76Ti where thinnest peaks are visible on MD simulation. Ti being the main element, it drives the phase formation. Peaks correspond to the β-Ti (BCC) phase that is not predicted by thermodynamics and not usually formed in typical magnetron sputtering deposition conditions. Nevertheless, from literature it is known that the β-Ti (BCC) phase may be obtained at lower temperature than 880 °C when a BCC stabilizing element is added. Fe, Cr, Cu, Ni, Co etc. have been identified as β-Ti (BCC) stabilizer[60,61]. Formation of this β-Ti (BCC) in the simulated film may stand for this stabilizing effect, since Cu low content is randomly mixed in Ti, and thus can act as impurity. It should be noted that simulating a pure Ti deposition leads to a HCP film (not represented here but written in table 2). Experimentally, different results are obtained, since the α-Ti (HCP) phase is detected, similarly to pure Ti film, in addition to a CuTi phase.

V. CONCLUSION

The crystalline structure of Cu-Zn and Cu-Ti-Zn films deposited by magnetron sputtering technique was analyzed by means of GIXRD and compared to predictions from three numerical methods.

First result is, that depending on the compositions around the equimolarity, the phase formed in binary Cu-Zn alloys is different: α-CuZn or γ-Cu_5Zn_8. When Ti is progressively added into the binary alloy, the Cu-Zn stabilized phase depends on the Cu/Zn ratio. Ti was found to be incorporated in this phase, inducing a modification of the corresponding lattice parameter and a loss of the crystallinity. For Ti percentages between 24 and 42 at.% amorphous or nano-crystalline phases are present.

Comparison with CALPHAD results highlights that for pure Ti or binary Cu-Zn films, the thermodynamically stable phases are formed in the films. Less agreement was found at low or high percentage of Ti introduced in the starting Cu-Zn system, and great differences were observed for compositions of the ternary alloy close to equimolarity. The fact that poorly ordered films are observed in the range 10-42 at. % of Ti is in line with the expected out-of-equilibrium nature of the magnetron sputter deposition method.

Only limited agreement was found between ML predictions and experiments. The main reason that can be invoked is the data base used to train the model that is based on bulk HEAs alloys.

This points out the fact that alloys in bulk or thin films do not behave in the same manner, and/or, that elaboration routes of bulk pieces are too different from that of thin films. Since bulk HEAs are usually synthesized using metallurgical methods including a quenching step, conditions could have been comparable to magnetron sputter deposition for which high cooling rates are reported. Our results suggest that this hypothesis is not valid. Developing an accurate ML approach would require building a dedicated data base. Regarding the growing interest for HEAs, MEAs (medium entropy alloys) and CCAs (complex concentrated alloys) thin film applications, this work would deserve to be done in the future.

MD simulations, using experimental energy distribution functions of film forming species as inputs, were expected to predict the phases experimentally obtained. The main result obtained from MD is the segregation of Zn and the formation of a Cu-Ti phase. This was not evidenced from the GIXRD analysis, but cannot completely be ruled out in poorly crystalline films. Since CALPHAD calculations anticipate the formation of Cu-Ti phases, this possibility has to be considered. A very good agreement is found between MD and GIXRD for peak position and shape for Ti at % between 10 and 42. The organization at the nanoscale cannot be determined from the implemented analysis for comparison. However, the general shape of simulated XRD patterns (see Figure 4), standing for the level of order in the film, is in good agreement with the experimental results for all the compositions. Our results highlight the crucial impact of the interaction potentials used in the calculations. This was well-known, but particularly pregnant in the case of the Cu-Zn system for which two different phases are thermodynamically stable at compositions around 50/50. All the results show the ability of MD simulations to give interesting trends but highlight the need to check the validity of the interaction potentials on some selected film/compositions.

ACKNOWLEDGMENTS

Conseil Régional Centre - Val de Loire is acknowledegded for supporting this work through grant ARD-MATEX #2021-00145829

AUTHOR DECLARATIONS

Conflict of interest

The authors have no conflicts to disclose.

Author contibutions

Dimitri Boivin: Investigation (lead); Writing/Original Draft Preparation (equal); Visualization (equal); Writing/Review & Editing (supporting).
Andrea Jagodar: Investigation (equal).
Pascal Brault: Conceptualization (equal); Investigation (supporting); Formal Analysis (lead); Funding Acquisition (supporting); Visualization (equal).
Thomas Vaubois: Investigation (supporting); Formal Analysis (equal); Writing/Review & Editing (equal); Visualization (equal).
Edern Menou: Investigation (supporting); Writing/Review & Editing (equal); Visualization (equal).
Barthelemy Aspe: Conceptualization (supporting); Visualization (supporting).
Amael Caillard: Conceptualization (supporting).
Pascal Andreazza: Conceptualization (supporting).
Marjorie Cavarroc-Weimer: Formal Analysis (equal); Writing/Review & Editing (equal); Funding Acquisition (supporting).
Anne-Lise Thomann: Conceptualization (equal); Funding Acquisition (lead); Project Administration (lead); Writing/Original Draft Preparation (lead).

REFERENCES

[1]D. Miracle and O. Senkov, "A critical review of high entropy alloys and related concepts," Acta Materialia **122**, 448–511 (2017).

[2]W. Zhang, P. K. Liaw, and Y. Zhang, "Science and technology in high-entropy alloys," Science China Materials **61**, 2–22 (2018).

[3]W. Li, P. Liu, and P. K. Liaw, "Microstructures and properties of high-entropy alloy films and coatings: a review," Materials Research Letters **6**, 199–229 (2018).

[4]E. Zhou, D. Qiao, Y. Yang, D. Xu, Y. Lu, J. Wang, J. A. Smith, H. Li, H. Zhao, P. K. Liaw, and F. Wang, "A novel Cu-bearing high-entropy alloy with significant antibacterial behavior against corrosive marine biofilms," Journal of Materials Science & Technology **46**, 201–210 (2020).

[5]Z. Li, D. Qiao, Y. Xu, E. Zhou, C. Yang, X. Yuan, Y. Lu, J.-D. Gu, S. Wolfgang, D. Xu, and F. Wang, "Cu-bearing high-entropy alloys with excellent antiviral properties," Journal of Materials Science & Technology **84**, 59–64 (2021).

[6]V. Govind, S. Bharadwaj, M. R. Sai Ganesh, J. Vishnu, K. V. Shankar, B. Shankar, and R. Rajesh, "Antiviral properties of copper and its alloys to inactivate covid-19 virus: a review," BioMetals **34**, 1217–1235 (2021).

[7]V. Stranak, H. Wulff, H. Rebl, C. Zietz, K. Arndt, R. Bogdanowicz, B. Nebe, R. Bader, A. Podbielski, Z. Hubicka, and R. Hippler, "Deposition of thin titanium–copper films with antimicrobial effect by advanced magnetron sputtering methods," Materials Science and Engineering: C **31**, 1512–1519 (2011).

[8]J. Mostaghimi, L. Pershin, H. Salimijazi, M. Nejad, and M. Ringuette, "Thermal spray copper alloy coatings as potent biocidal and virucidal surfaces," Journal of Thermal Spray Technology **30**, 25–39 (2021).

[9]R. Li, L. Xie, W. Y. Wang, P. K. Liaw, and Y. Zhang, "High-Throughput Calculations for High-Entropy Alloys: A Brief Review," Frontiers in Materials **7** (2020), 10.3389/fmats.2020.00290.

[10]S. Guo, Q. Hu, C. Ng, and C. Liu, "More than entropy in high-entropy alloys: Forming solid solutions or amorphous phase," Intermetallics **41**, 96–103 (2013).

[11]S. Guo, Q. Hu, C. Ng, and C. Liu, "High-entropy alloys: A critical review," Materials Research Letters **2**, 107–123 (2014).

[12]E. Menou, I. Toda-Caraballo, P. E. J. Rivera-Díaz-del Castillo, C. Pineau, E. Bertrand, G. Ramstein, and F. Tancret, "Evolutionary design of strong and stable high entropy alloys using multi-objective optimisation based on physical models, statistics and thermodynamics," Materials & Design **143**, 185–195 (2018).

[13]J. Yu, F. Yu, Q. Fu, G. Zhao, C. Gong, M. Wang, and Q. Zhang, "Combining Machine Learning and Molecular Dynamics to Predict Mechanical Properties and Microstructural Evolution of FeNiCrCoCu High-Entropy Alloys," Nanomaterials **13**, 968 (2023).

[14]E. Woods, C. Cochrane, and S. Percival, "Prevalence of silver resistance genes in bacteria isolated from human and horse wounds," Veterinary Microbiology **138**, 325–329 (2009).

[15]C. Popescu, S. Alain, M. Courant, A. Vardelle, A. Denoirjean, and M. Cavarroc, "Thermal spray copper-based coatings against contamination of thermoplastic surfaces: A systematic review," Engineering Science and Technology, an International Journal **35**, 101194 (2022).

[16]A. M. N. Saunders, ed., in *CALPHAD: Calculation of Phase Diagrams - A Comprehensive Guide* (Elsevier, 1998) p. 1–4.

[17]P. Brault, A.-L. Thomann, and M. Cavarroc, "Theory and molecular simulations of plasma sputtering, transport and deposition processes," The European Physical Journal D **77** (2023), 10.1140/epjd/s10053-023-00592-x.

[18]L. Xie, P. Brault, A.-L. Thomann, and L. Bedra, "Molecular dynamic simulation of binary ZrxCu100-x metallic glass thin film growth," Applied Surface Science **274**, 164–170 (2013).

[19]S. Atmane, A. Maroussiak, A. Caillard, A.-L. Thomann, M. Kateb, J. T. Gudmundsson, and P. Brault, "Role of sputtered atom and ion energy distribution in films deposited by physical vapor deposition: A molecular dynamics approach," Journal of Vacuum Science & Technology A **42**, 060401 (2024), https://pubs.aip.org/avs/jva/article-pdf/doi/10.1116/6.0004134/20256147/060401_1_6.0004134.pdf.

[20]L. Xie, P. Brault, A.-L. Thomann, and J.-M. Bauchire, "AlCoCrCuFeNi high entropy alloy cluster growth and annealing on silicon: A classical molecular dynamics simulation study," Applied Surface Science **285**, 810–816 (2013).

[21]L. Xie, P. Brault, A.-L. Thomann, X. Yang, Y. Zhang, and G. Shang, "Molecular dynamics simulation of Al–Co–Cr–Cu–Fe–Ni high entropy alloy thin film growth," Intermetallics **68**, 78–86 (2016).

[22]Conditions Extrêmes et Matériaux : Haute Température et Irradiation, UPR3079 CNRS, CS 30058, 3A rue de la Férollerie, F-45071 Orléans, France.

[23]M. Mayer, *SIMNRA User's Guide , Report IPP 9/113* (Max-Planck-Institut für Plasmaphysik, Garching, Germany, 1997).

[24]M. S. Daw and M. I. Baskes, "Embedded-atom method: Derivation and application to impurities, surfaces, and other defects in metals," Physical Review B **29**, 6443–6453 (1984).

[25]R. A. Johnson, "Alloy models with the embedded-atom method," Physical Review B **39**, 12554–12559 (1989).

[26]X. W. Zhou, R. A. Johnson, and H. N. G. Wadley, "Misfit-energy-increasing dislocations in vapor-deposited CoFe/NiFe multilayers," Physical Review B **69** (2004), 10.1103/physrevb.69.144113.

[27]J. Tersoff, "Empirical interatomic potential for silicon with improved elastic properties," Physical Review B **38**, 9902–9905 (1988).

[28]D. W. Jacobson and G. B. Thompson, "Revisting Lennard Jones, Morse, and N-M potentials for metals," Computational Materials Science **205**, 111206 (2022).

[29]L. Zhang and S. Jiang, "Molecular simulation study of nanoscale friction for alkyl monolayers on Si(111)," The Journal of Chemical Physics **117**, 1804–1811 (2002).

[30]L. Xie, P. Brault, J.-M. Bauchire, A.-L. Thomann, and L. Bedra, "Molecular dynamics simulations of clusters and thin film growth in the context of plasma sputtering deposition," Journal of Physics D: Applied Physics **47**, 224004 (2014).

[31]J. P. Biersack, M. D. Ziegler, and Ziegler, *The Stopping and Range of Ions in Matter, ISBN: 9780965420716* (SRIM Company, Chester, MD, USA, 2008).

[32]A. P. Thompson, H. M. Aktulga, R. Berger, D. S. Bolintineanu, W. M. Brown, P. S. Crozier, P. J. in 't Veld, A. Kohlmeyer, S. G. Moore, T. D. Nguyen, R. Shan, M. J. Stevens, J. Tranchida, C. Trott, and S. J. Plimpton, "LAMMPS - a flexible simulation tool for particle-based materials modeling at the atomic, meso, and continuum scales," Computer Physics Communications **271**, 108171 (2022).

[33]"LAMMPS Software Homepage," Available at `https://www.lammps.org` (2023), (last visited 2024/08/23).

[34]S. P. Coleman, D. E. Spearot, and L. Capolungo, "Virtual diffraction analysis of Ni [010] symmetric tilt grain boundaries," Modelling and Simulation in Materials Science and Engineering **21**, 055020 (2013).

[35]A. Stukowski, "Visualization and analysis of atomistic simulation data with OVITO–the Open Visualization Tool," Modelling and Simulation in Materials Science and Engineering **18**, 015012 (2009).

[36]K. Lee, M. V. Ayyasamy, P. Delsa, T. Q. Hartnett, and P. V. Balachandran, "Phase classification of multi-principal element alloys via interpretable machine learning," npj Computational Materials **8** (2022), 10.1038/s41524-022-00704-y.

[37]T. Chen and C. Guestrin, "XGBoost: A Scalable Tree Boosting System," in *Proceedings of the 22nd ACM SIGKDD International Conference on Knowledge Discovery and Data Mining*, KDD

'16 (ACM, 2016).

[38]"Thermo-Calc Software AB," Available at `http://www.thermocalc.com/` (2023), (last visited 2024/08/23).

[39]Y. Tang, J. Ma, D. Han, J. Wang, H. Qi, and L. Jin, "Critical Evaluation and Thermodynamic Optimization of the Cu-Zn, Cu-Se and Zn-Se Binary Systems," Metals **12**, 1401 (2022).

[40]J.-J. Tian, K. Wang, K.-W. Xu, X.-T. Luo, G.-S. Shao, and C.-J. Li, "Effect of coating composition on the micro-galvanic dissolution behavior and antifouling performance of plasma-sprayed laminated-structured Cu Ti composite coating," Surface and Coatings Technology **410**, 126963 (2021).

[41]P. Zeman, S. Haviar, and M. Červená, "Self-formation of dual glassy-crystalline structure in magnetron sputtered W–Zr films," Vacuum **187**, 110099 (2021).

[42]E. Lugscheider, C. Barimani, C. Wolff, S. Guerreiro, and G. Doepper, "Comparison of the structure of PVD-thin films deposited with different deposition energies," Surface and Coatings Technology **86–87**, 177–183 (1996).

[43]R. Mareus, C. Mastail, F. Angay, N. Brunetière, and G. Abadias, "Study of columnar growth, texture development and wettability of reactively sputter-deposited TiN, ZrN and HfN thin films at glancing angle incidence," Surface and Coatings Technology **399**, 126130 (2020).

[44]M. A. Borysiewicz, P. Barańczyk, J. Zawadzki, M. Wzorek, R. Zybała, B. Synkiewicz-Musialska, and P. Krzyściak, "Nanoporous copper films: How to grow porous films by magnetron sputter deposition," Crystals **14** (2024).

[45]S. Kabekkodu, A. Dosen, and B. T., "Pdf-5+ : a comprehensive powder diffraction file for materials characterization." Powder Diffraction **39**, 47–59 (2024).

[46]A. Jain, S. P. Ong, G. Hautier, W. Chen, W. D. Richards, S. Dacek, S. Cholia, D. Gunter, D. Skinner, G. Ceder, and K. A. Persson, "Commentary: The Materials Project: A materials genome approach to accelerating materials innovation," APL Materials **1**, 011002 (2013), https://pubs.aip.org/aip/apm/article-pdf/doi/10.1063/1.4812323/13163869/011002_1_online.pdf.

[47]"Materials project homepage homepage," Available at `https://next-gen.materialsproject.org/` (2023), (last visited 2024/08/23).

[48]M. Kowalski and P. J. Spencer, "Thermodynamic reevaluation of the Cu-Zn system," Journal of Phase Equilibria **14**, 432–438 (1993).

[49]J. Wang, H. Xu, S. Shang, L. Zhang, Y. Du, W. Zhang, S. Liu, P. Wang, and Z.-K. Liu, "Experimental investigation and thermodynamic modeling of the Cu–Si–Zn system with the refined description for the Cu–Zn system," Calphad **35**, 191–203 (2011).

[50]W. Gierlotka and S.-w. Chen, "Thermodynamic descriptions of the Cu–Zn system," Journal of Materials Research **23**, 258–263 (2008).

[51]S.-M. Liang, H.-M. Hsiao, and R. Schmid-Fetzer, "Thermodynamic assessment of the Al–Cu–Zn system, part I: Cu–Zn binary system," Calphad **51**, 224–232 (2015).

[52]H. Okamoto, M. Schlesinger, and E. Mueller, *Alloy Phase Diagrams* (ASM International, 2016).

[53]H.-W. Chen, K.-C. Hsu, Y.-C. Chan, J.-G. Duh, J.-W. Lee, J. S.-C. Jang, and G.-J. Chen, "Antimicrobial properties of Zr–Cu–Al–Ag thin film metallic glass," Thin Solid Films **561**, 98–101 (2014).

[54]Y. Liu, J. Padmanabhan, B. Cheung, J. Liu, Z. Chen, B. E. Scanley, D. Wesolowski, M. Pressley, C. C. Broadbridge, S. Altman, U. D. Schwarz, T. R. Kyriakides, and J. Schroers, "Combinatorial development of antibacterial Zr-Cu-Al-Ag thin film metallic glasses," Scientific Reports **6** (2016), 10.1038/srep26950.

[55]Y. Jeyachandran, B. Karunagaran, S. Narayandass, D. Mangalaraj, T. Jenkins, and P. Martin, "Properties of titanium thin films deposited by dc magnetron sputtering," Materials Science and Engineering: A **431**, 277–284 (2006).

[56]J. Musil and J. Vlček, "Magnetron sputtering of films with controlled texture and grain size," Materials Chemistry and Physics **54**, 116–122 (1998), symposium H of the 4th IUMRS International Conference in Asia.

[57]P. Keuter, M. to Baben, S. Aliramaji, and J. M. Schneider, "CALPHAD-Based Modelling of the Temperature–Composition–Structure Relationship during Physical Vapor Deposition of Mg-Ca Thin Films," Materials **16**, 2417 (2023).

[58]F. Cemin, M. J. Jimenez, L. M. Leidens, C. A. Figueroa, and F. Alvarez, "A thermodynamic study on phase formation and thermal stability of AlSiTaTiZr high-entropy alloy thin films," Journal of Alloys and Compounds **838**, 155580 (2020).

[59]J.-C. Ren, J. Zhou, C. J. Butch, Z. Ding, S. Li, Y. Zhao, and W. Liu, "Predicting single-phase solid solutions in as-sputtered high entropy alloys. high-throughput screening with machine-learning model," Journal of Materials Science and Technology **138**, 70–79 (2023).

[60]R. P. Kolli and A. Devaraj, "A Review of Metastable Beta Titanium Alloys," Metals **8**, 506 (2018).

[61]P. Pesode and S. Barve, "A review—metastable β titanium alloy for biomedical applications," Journal of Engineering and Applied Science **70** (2023), 10.1186/s44147-023-00196-7.